Tuning of Electrocatalytic Characteristics of PANI/Fe_2O_3 Composite Coating for Alkaline Hydrogen Evolution Reaction

V. S. Sumi,[a] Liju Elias,[a] M. J. Deepa,[a] S. M. A. Shibli*[a,b]

[a]*Department of Chemistry, University of Kerala, Kariavattom Campus, Thiruvananthapuram, Kerala–695 581, India*

[b]*Centre for Renewable Energy and Materials, University of Kerala, Kariavattom Campus, Thiruvananthapuram, Kerala–695 581, India*

E-mail: *smashibli@yahoo.com, Phone: +91 471 2308682 (Off) +91 85470 67230 (Mob)

Supporting Information

1. Results and discussion

1.1 Characterization of PANI/Fe_2O_3 composite

1.1.1 Confirmation of the crystalline phase of PANI/Fe_2O_3 composite

XRD studies were carried out to understand the phase structure and crystallinity of PANI/Fe_2O_3 composite. Composition of the synthesized composite was optimized by analyzing the results of XRD patterns of various compositions of PANI/Fe_2O_3 say PANI/Fe_2O_3 (1:0.5), PANI/Fe_2O_3 (1:1) and PANI/Fe_2O_3 (1:2). The XRD patterns of the different composites are compared with pure PANI in **Fig. S1**. A broad diffraction peak centered at $2\theta = 25.3^{\circ}$ is observed in the XRD pattern of pure PANI and can be attributed to (110) plane of amorphous PANI in accordance with the other reports [29,30]. The present composites exhibit peaks of both PANI and Fe_2O_3. In all the composites, an XRD peak at $2\theta = 25^{\circ}$ indicating the presence of PANI in the composites. The crystalline peaks observed at 24.4°, 33.2°, 35.7°, 40.8°, 45.8°, 54.1°, 64.1°and 72.1° correspond to (012), (104), (110), (113), (024), (116), (300) and (220) planes of hexagonal Fe_2O_3 (JCPDS 33-

0664) [31,32]. PANI/Fe_2O_3 (1:1) exhibits intense peaks due to its high crystallinity and different crystal phases are clearly noted. This ratio was selected as the optimum for further studies. The crystalline size of the polymer composite calculated using Scherrer formula was 120 nm. For explaining the catalytic properties of the composite, it was essential to account the type of bonding present in the synthesized composite along with its electronic and molecular structures.

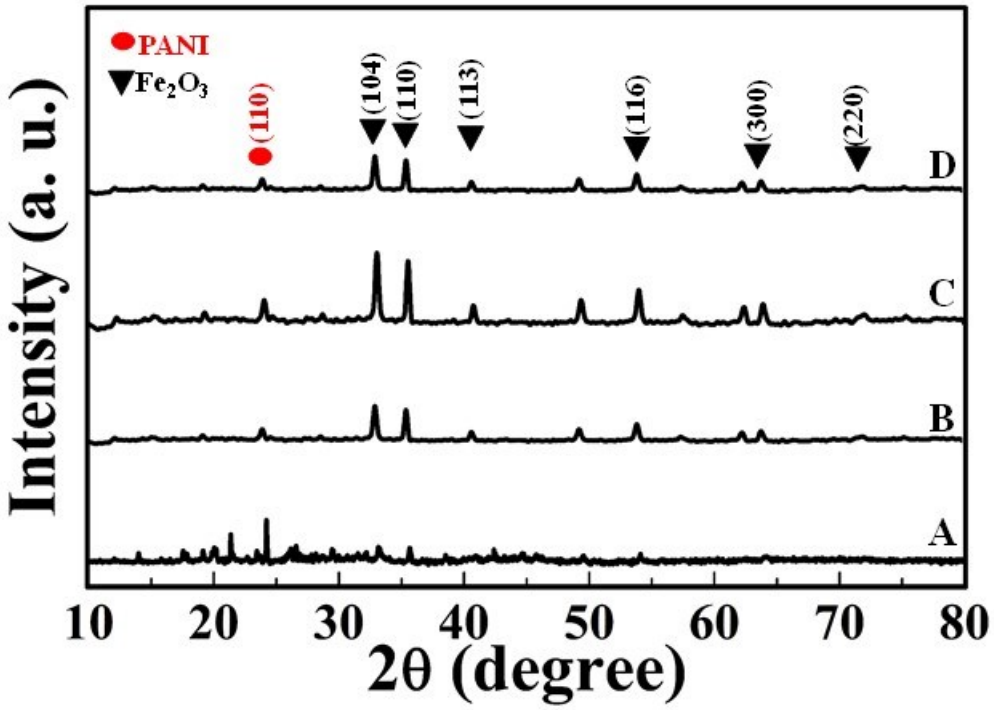

Fig. S1: XRD patterns of the synthesized samples: A) PANI, B) 1:0.5 PANI/Fe_2O_3, C) 1:1 PANI/Fe_2O_3 and D) 1:2 PANI/Fe_2O_3

1.1.2 Confirmation of optical property of PANI/Fe_2O_3

The optical properties of the synthesized PANI and PANI/Fe_2O_3 composite were carried out by UV- Visible spectra recorded from 200 nm to 800 nm range. The absorption edge of both pure PANI and PANI/Fe_2O_3 are represented in **Fig. S2**. The peak observed at 315 nm can be attributed to π - π* transition of benzenoid units in polyaniline and peak at 646 nm can be attributed to exciton

like transition in quinonic diimino units. A peak at 415 nm present in the UV - Visible spectrum is due to the localized polarons characterized by protonated polyaniline [33,34]. The catalytic activity of the composite greatly depends on the synergistic interaction among the individual constituents. UV- Visible spectrum of PANI/Fe_2O_3 composite exhibits three absorption peaks at 280 nm, 580 nm and 780 nm. The peak, at 280 nm is due to the π - π* transition of the benzenoid ring, at 580 nm can be attributed to the quinolic excitonic transition, and the peak at 780 nm is due to the π polaron transition. The enhanced catalytic activity in the present PANI/Fe_2O_3 composite is due to the interaction between highly conjugated PANI and the inorganic metal oxide.

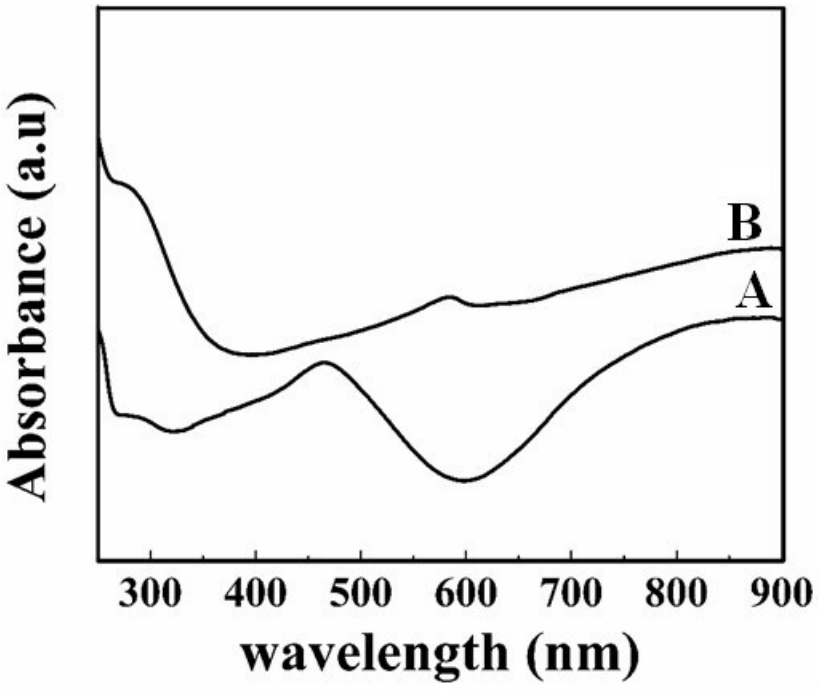

Fig. S2: A) UV-visible absorption spectra of: A) PANI and B) PANI/Fe_2O_3 composite

1.1.3 Confirmation of bonding characteristics of PANI/Fe_2O_3 composite

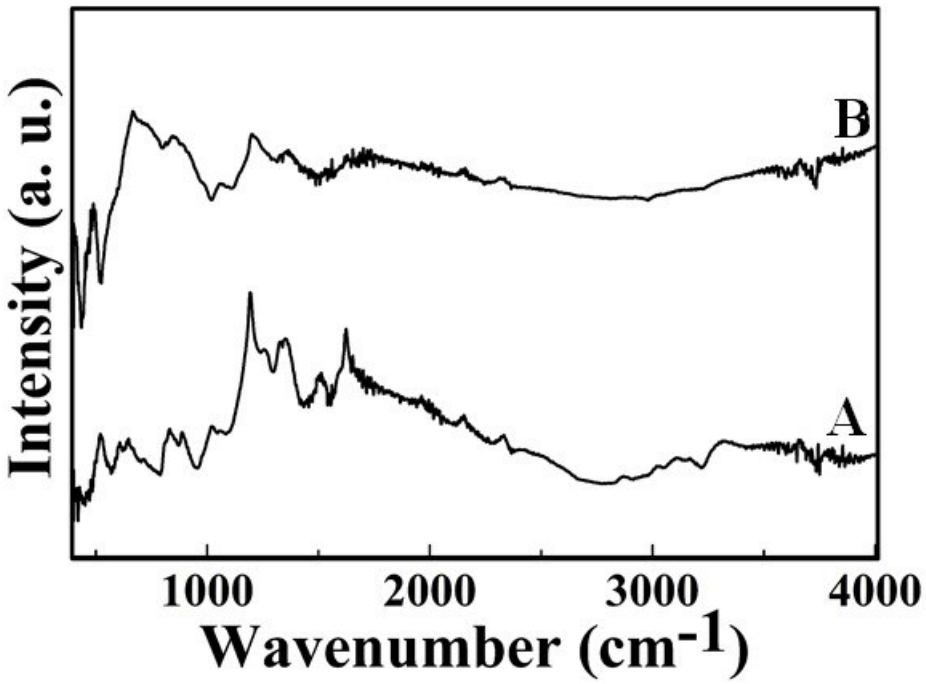

Fig. S3: FTIR spectra of a) PANI b) PANI/Fe_2O_3 composite

The analysis provides information about the vibrational excitations and interaction of radiation with free carriers present in the conducting polymer. The molecular structure and the bonding characteristics of the synthesized PANI and PANI/Fe_2O_3 composite are studied by FTIR (recorded in 400 cm^{-1} to 4000 cm^{-1} with a spectral resolution at a minimum of 4 cm^{-1}) spectroscopy and the corresponding spectra are shown in **Fig. S3a**. The FTIR spectrum of PANI exhibits peak at 1294 cm^{-1} corresponding to the C–N stretching modes of the leuco emaraldene structure of PANI. The peak at 1130 cm^{-1} is due to the C–H bending mode of aniline and that at 1244 cm^{-1} is related to the protonated C–N group i.e., as C–NH^+. The characteristic peaks at 1492 cm^{-1} and 1578 cm^{-1} are assigned to the C=C stretching modes of the benzenoid ring and quinoid ring respectively. This spectral results indicate that the state of the polyaniline is emaraldene rather than solely the leuco

emaraldene. The metal oxide bond and functional groups in the present PANI/Fe_2O_3 composite is studied from FTIR spectral results (**Fig. S3b**). The peak at 587 cm^{-1} corresponds to the bending mode of Fe–O. The peak at 3400 cm^{-1} corresponds to the hydrogen bonds in water [35]. The peak at 3440 cm^{-1} can be assigned to stretching vibrations of O–H. The peak at 1573 cm^{-1} is due to C–C stretching vibrations of the quinoid ring and the peak at 1496 cm^{-1} is due to the vibrations of the benzenoid ring in the composite [36]. The peak at 1565 cm^{-1} can be ascribed to the characteristic bond of nitrogen quinone structure [37] and the peak at 1406 cm^{-1} indicate the characteristic of the N–H bonding deformation of the protonated amine [38]. The band at 1300 cm^{-1} is assigned to the stretching of the C – N bonds of the aromatic amines. Broad bands observed in the range of 600 – 800 cm^{-1} is due to Fe–O vibration. The characteristic peaks of both PANI and Fe_2O_3 found in the spectrum of the nanocomposite confirmed the successful incorporation of the metal oxide into the polymer matrix.

1.1.4 Evidence for the decrease in particle size on composite formation

The particle size distribution of the synthesized composite is very important for analyzing the uniformity in size distribution of the particles. The measurement of zeta potential is also important for expressing the stability of the synthesized particles since it is used for catalytic applications. **Fig. S4a** shows the size distribution curve obtained from DLS studies of PANI and PANI/Fe_2O_3 composite. The average particle size of PANI and PANI/Fe_2O_3 are 410 nm and 360 nm respectively and the size are quite larger than the size obtained from TEM and SEM analyses. This can be attributed to the swelling of the particles in the aqueous medium. The size measured from the DLS is actually the hydrodynamic size of the particle. The potential distribution curves of PANI and PANI/Fe_2O_3 composite are shown in **Fig. S4b**. The zeta potential values of PANI and

PANI/Fe_2O_3 composite are 0.3 mV and 5.8 mV, respectively. The high zeta potential of the composite confirmed the high surface charge of the particles. The particles remains as suspended form in solution which extends its high catalytic efficiency [38,40].

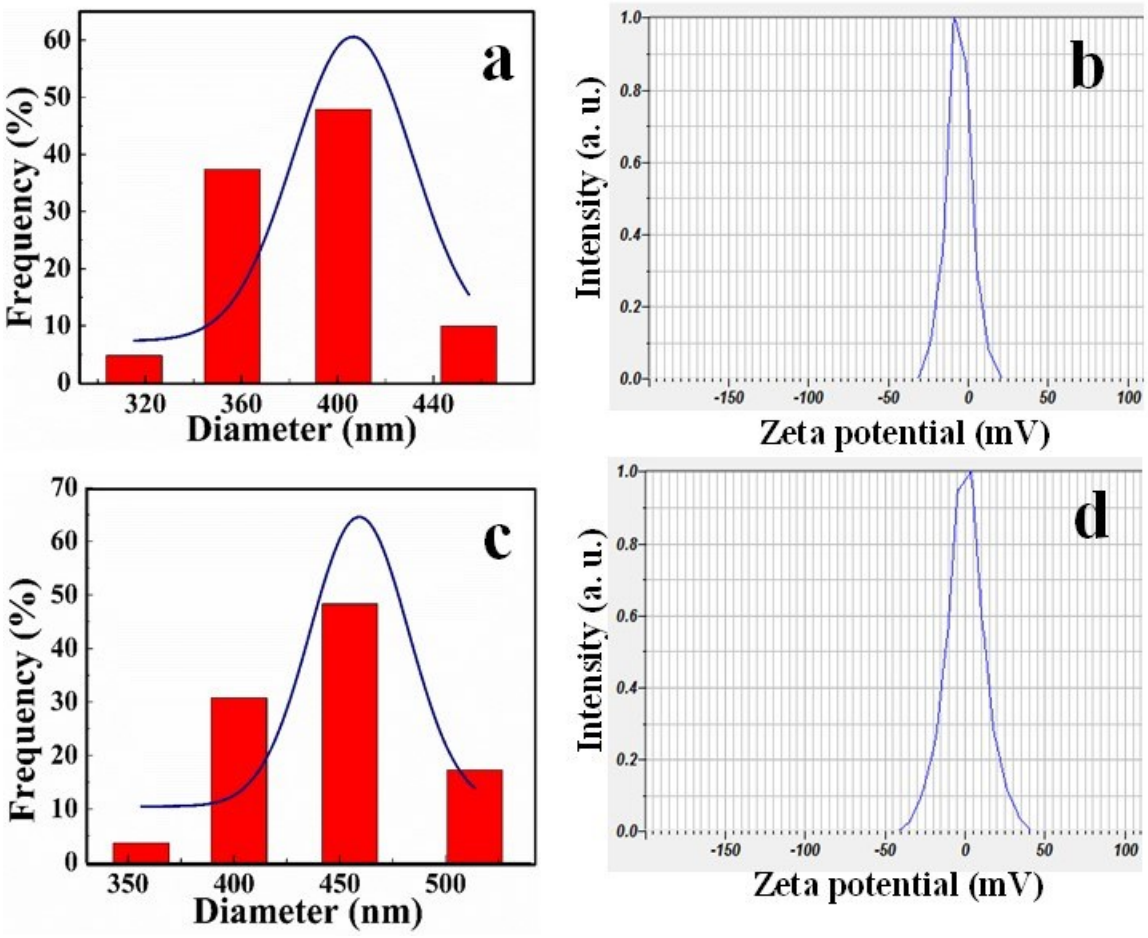

Fig. S4: a) DLS and b) Zeta potential of PANI c) DLS and d) Zeta potential of PANI/Fe2O3 composite

1.1.5 Morphology and distribution of the particle

The micrographs of PANI and PANI/Fe_2O_3 composites are shown in **Fig. S5**. PANI exhibits irregularly distributed cauliflower like structures with the interconnected particles of nano dimensions. The SEM images of PANI/Fe_2O_3 composite show irregular rod shaped Fe_2O_3 particles distributed unevenly in the PANI polymer matrix. The 500 nm long rods having width 50 – 150

nm are distributed over the matrix. A few spherical agglomerates are also observed. The SEM micrographs of PANI and PANI/Fe_2O_3 nanocomposites indicate the formation of rough microstructure having agglomerated clusters of Fe_2O_3 nested in the PANI/Fe_2O_3 polymer matrix. The surface of the matrix is porous in nature which is an essential requirement of an electrocatalyst.

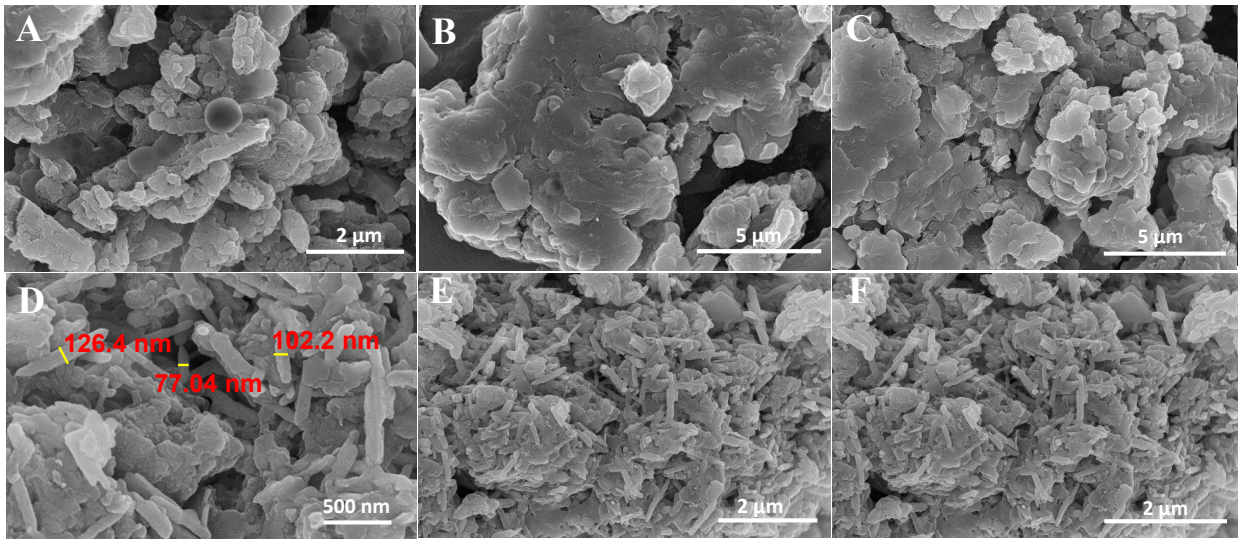

Fig. S5: FESEM image of (**A–C**) PANI and (D–F) PANI/Fe_2O_3 composite at different magnifications

The elemental compositions of the synthesized composite was confirmed from EDS analysis. The obtained spectra and elemental mapping results of PANI and PANI/Fe_2O_3 composite are shown in **Fig. S6** and **Fig. S7**, respectively. The percentage compositions of all the elements in PANI and PANI/Fe_2O_3 are represented in **Table S1**. It is observed from the spectrum that the major elements present in PANI are carbon and nitrogen. In the present PANI/Fe_2O_3 composite, the major elements are carbon, nitrogen, iron and oxygen. The EDS mapping of PANI and PANI/Fe_2O_3 composite and the elemental distribution of each species are shown in **Fig. S6** and **Fig. S7**, respectively. Mapping results confirm that the elements are uniformly distributed in PANI and PANI/Fe_2O_3 composite.

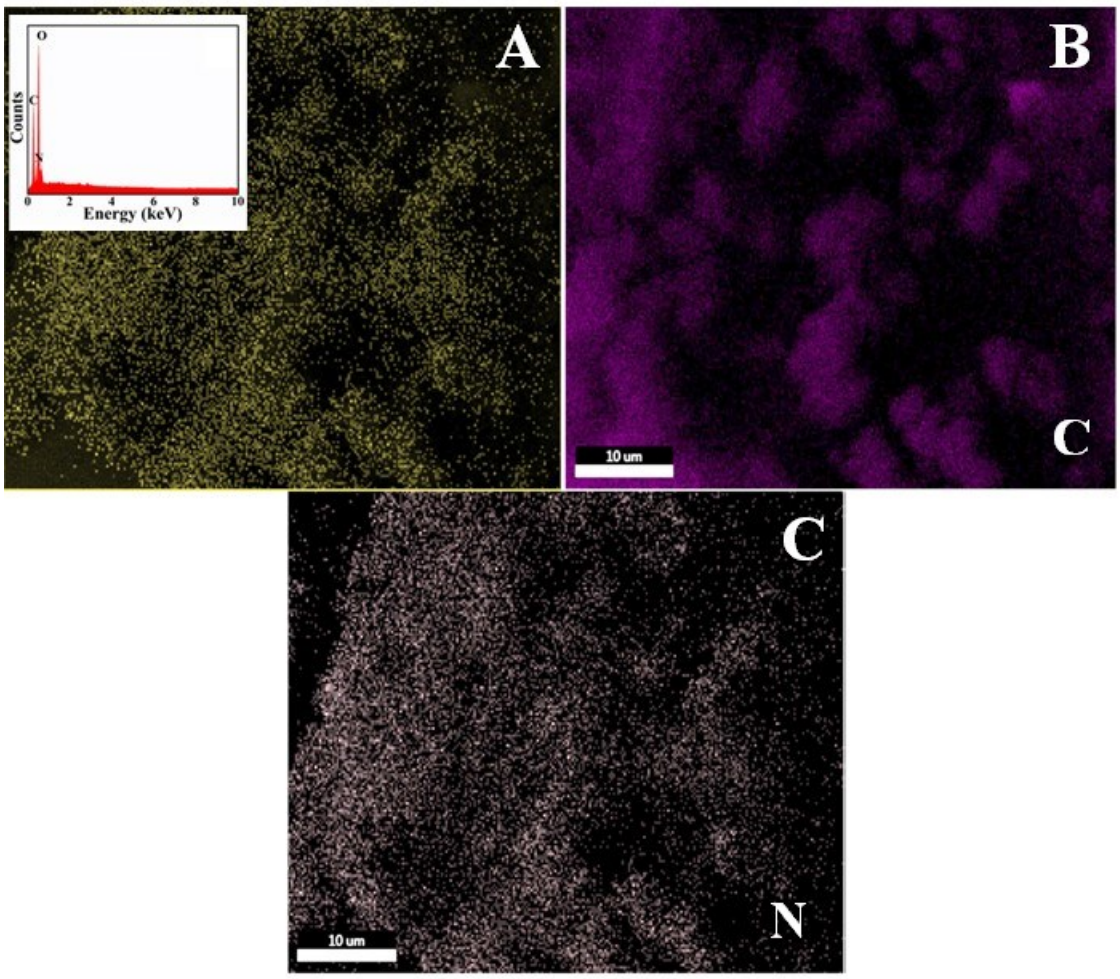

Fig. S6: EDAX elemental mapping results of pure PANI: A) all elements along with EDS spectrum in the inset, B) Carbon and C) Nitrogen

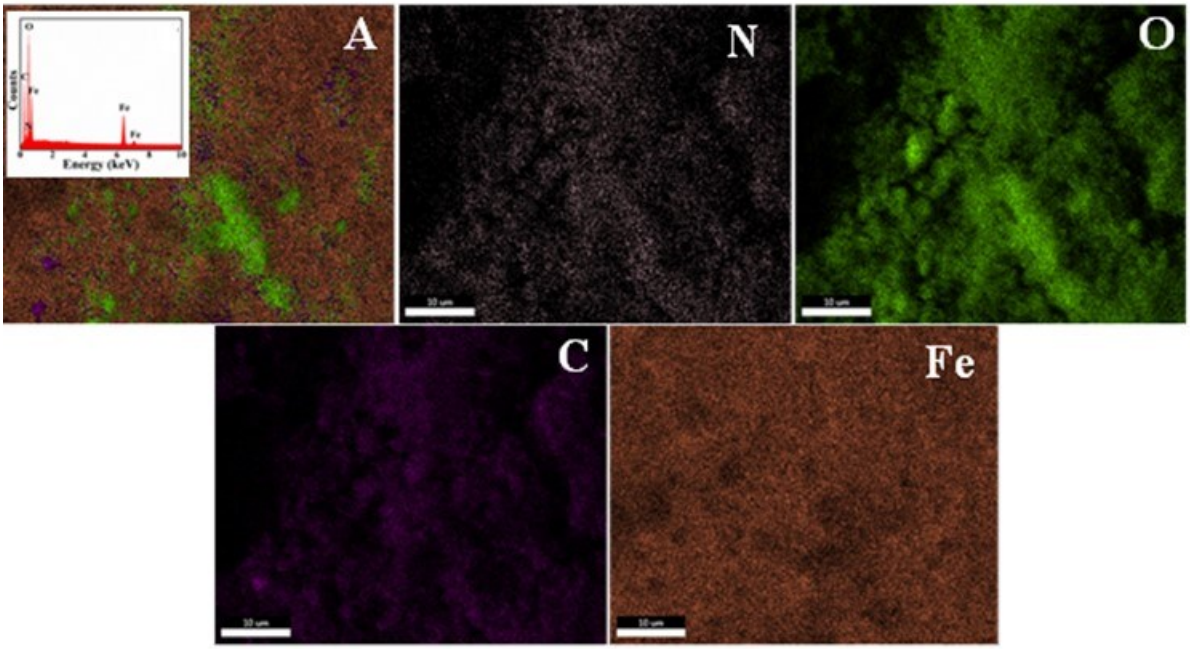

Fig. S7: EDAX mapping images of **A**) PANI//Fe_2O_3 composite with EDAX spectrum in the inset and elemental mapping images of **N**) Nitrogen, **O**) Oxygen, **C**) Carbon and **Fe**) Iron

Table S1: Surface elemental compositions of the synthesized particles from EDAX analysis

Composite	**Weight percentage of elements in the synthesized compound**			
	Carbon	Nitrogen	Iron	Oxygen
PANI	82.12	17.88	0	0
Pani/Fe_2O_3	31.02	21.63	12.51	34.84

1.2 Characterization of PANI/Fe_2O_3 composite coatings

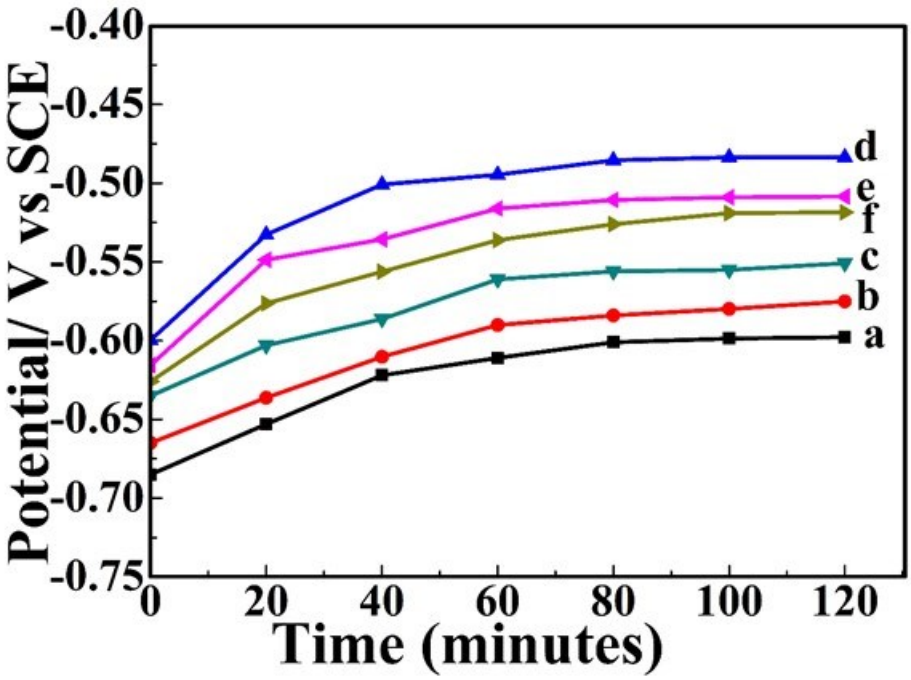

Fig. S8: potential of deposition curves of a) Bare NiP b) PANI–NiP coating c) PANI/Fe_2O_3–NiP1GL d) PANI/Fe_2O_3–NiP2GL e) PANI/Fe_2O_3–NiP5GL f) PANI/Fe_2O_3–NiP10GL

Table S2: Physical characteristics of various compositions of the developed PANI/Fe_2O_3 incorporated NiP coating

Coatings	Thickness (µm)	Hardness (VHN)	Porosity
Bare NiP	15	500	Less porous
Bare PANI	17	501	More porous
PANI/Fe_2O_3–1GL	20	503	More porous
PANI/Fe_2O_3–2GL	26	510	More porous
PANI/Fe_2O_3–5GL	24	506	More porous
PANI/Fe_2O_3–10GL	22	504	More porous

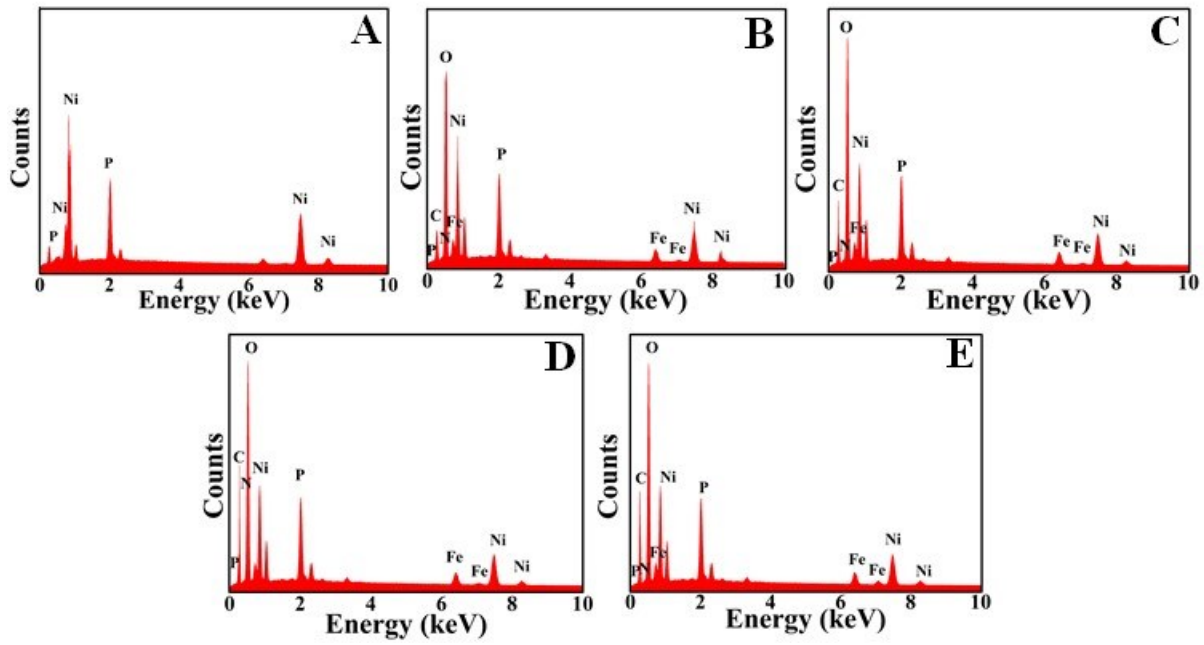

Fig. S9: EDAX spectra of the developed coatings A) Bare NiP, B) PANI/Fe_2O_3–1GL, C) PANI/Fe_2O_3–2GL, D) PANI/Fe_2O_3–5GL and E) PANI/Fe_2O_3–10GL

Table S3: Surface elemental compositions of PANI/Fe_2O_3 incorporated NiP coating from EDS analysis

Composite	**Weight percentage of elements in the developed coatings**					
	Nickel	**Phosphorous**	**Carbon**	**Nitrogen**	**Iron**	**Oxygen**
Bare NiP	88.11	11.89	0	0	0	0
Bare PANI	58.34	10.51	8.05	4.16	0	7.28
PANI/Fe_2O_3–1GL	61.07	11.07	8.94	3.86	1.74	13.32
PANI/Fe_2O_3–2GL	54.92	10.58	9.85	4.15	2.04	18.46
PANI/Fe_2O_3–5GL	52.17	10.02	10.25	4.54	2.24	20.78
PANI/Fe_2O_3–10GL	48.29	9.73	11.92	4.93	2.37	22.76

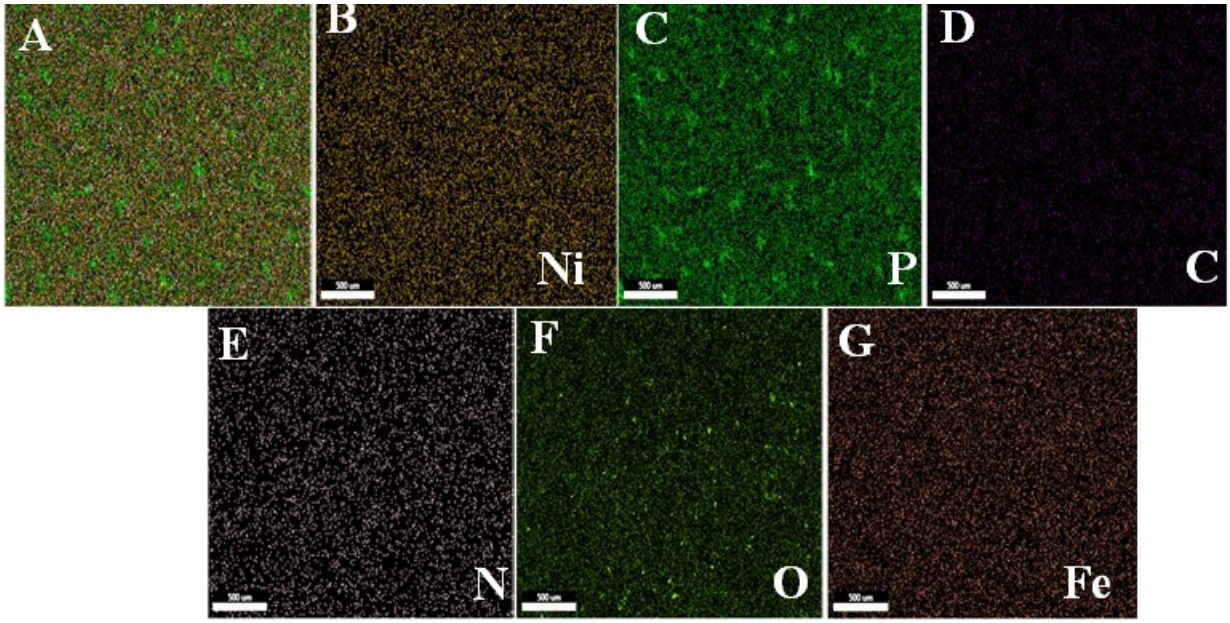

Fig. S10: EDAX mapping images of A) PANI/Fe_2O_3–NiP coating and (B to G) the various elements in the coating Nickel, Phosphorous, Carbon, Nitrogen, Oxygen and Iron, respectively

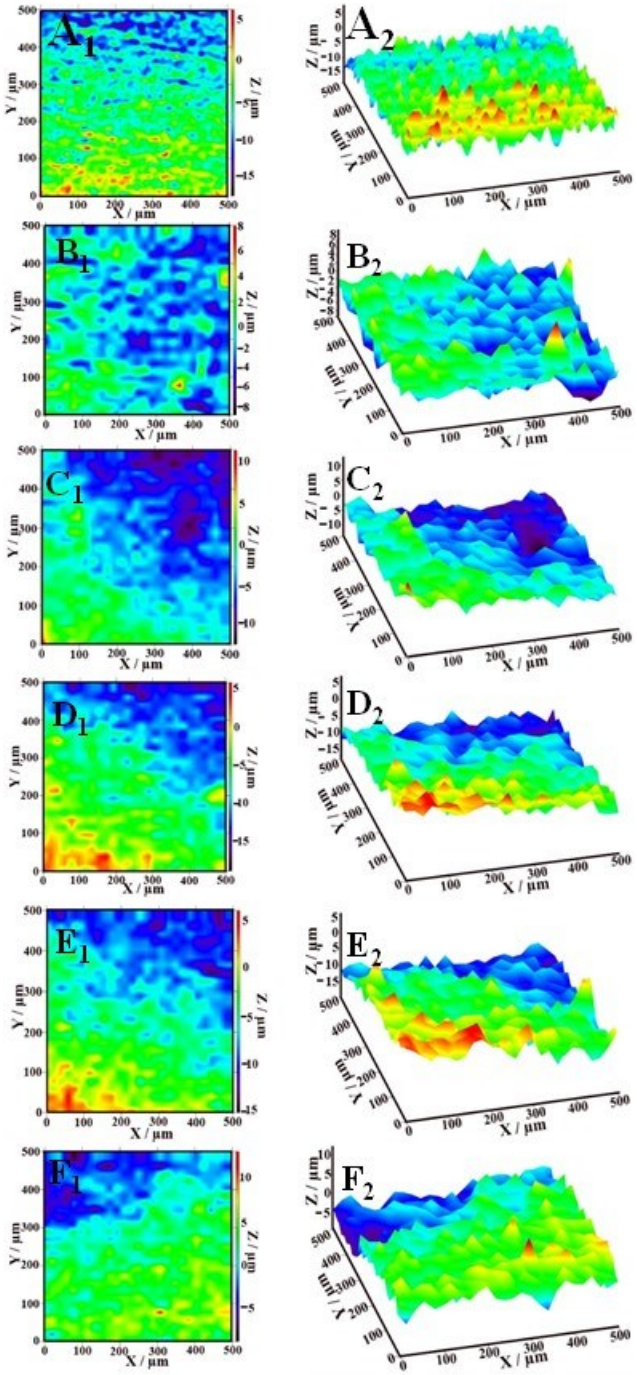

Fig. S11: 2D and 3D Optical surface profiles of the developed coatings: A) Bare NiP, B) Bare PANI, C) PANI/Fe_2O_3–1GL, D) PANI/Fe_2O_3–2GL, E) PANI/Fe_2O_3–5GL and F) PANI/Fe_2O_3–10GL

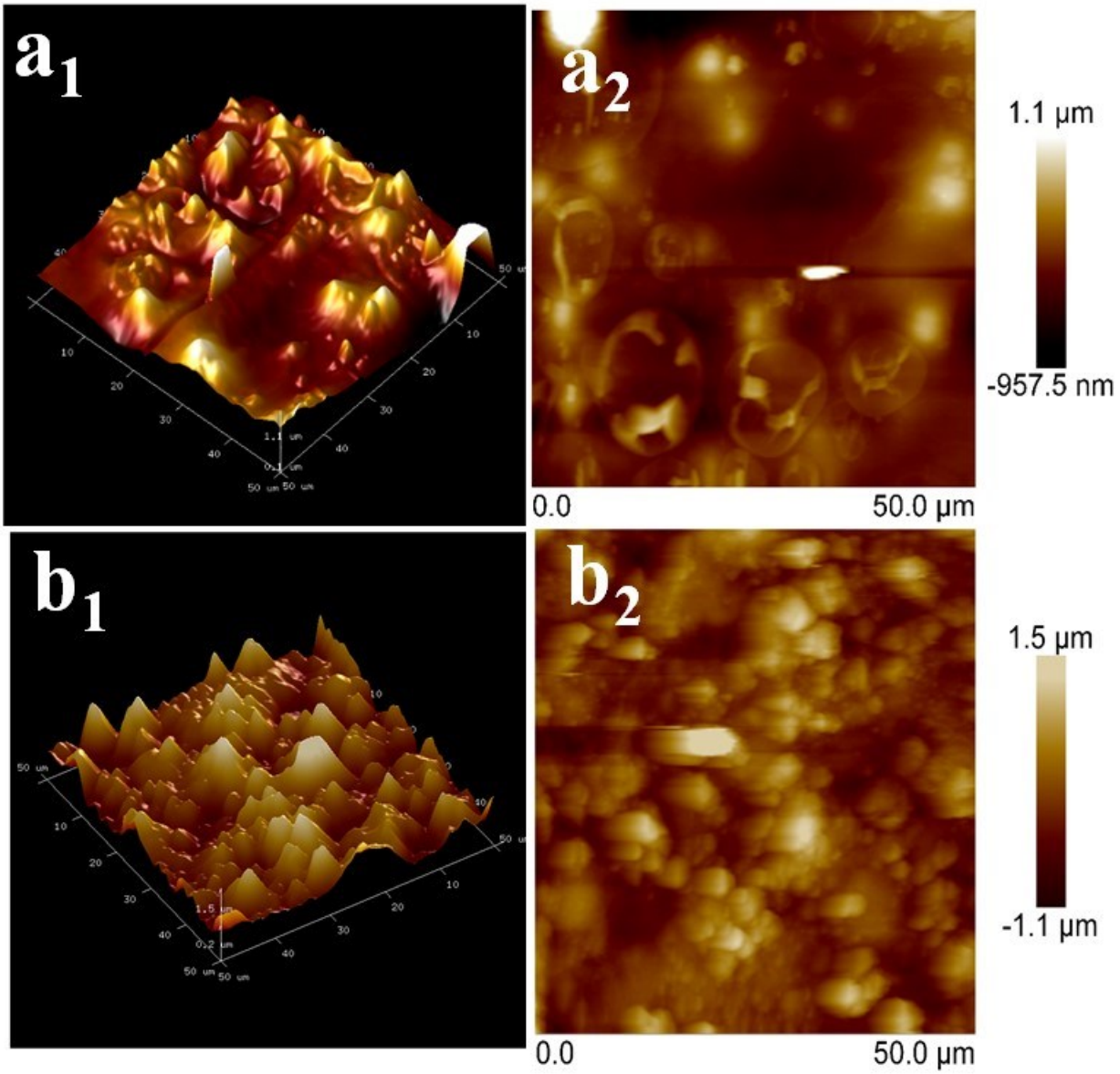

Fig. S12: AFM images of the developed coatings: (**a_1** & **a_2**) Bare NiP and (**b_1** & **b_2**) PANI/Fe_2O_3–2GL coating

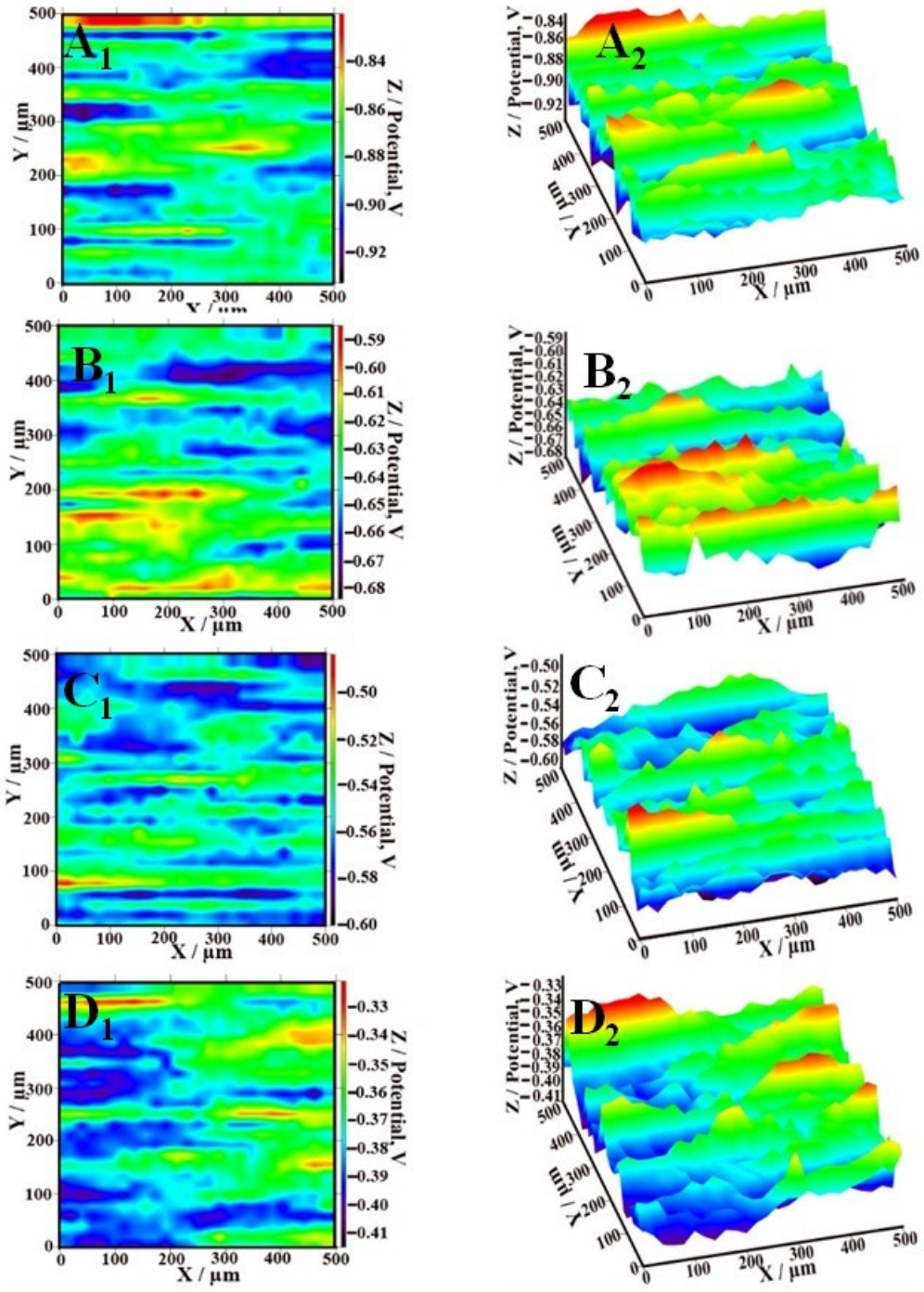

Fig. S13: 2D and 3D SKPM images of A) PANI–NiP, B) PANI/Fe_2O_3–NiP 1GL, C) PANI/Fe_2O_3–NiP 5GL and D) PANI/Fe_2O_3–NiP 10GL coatings

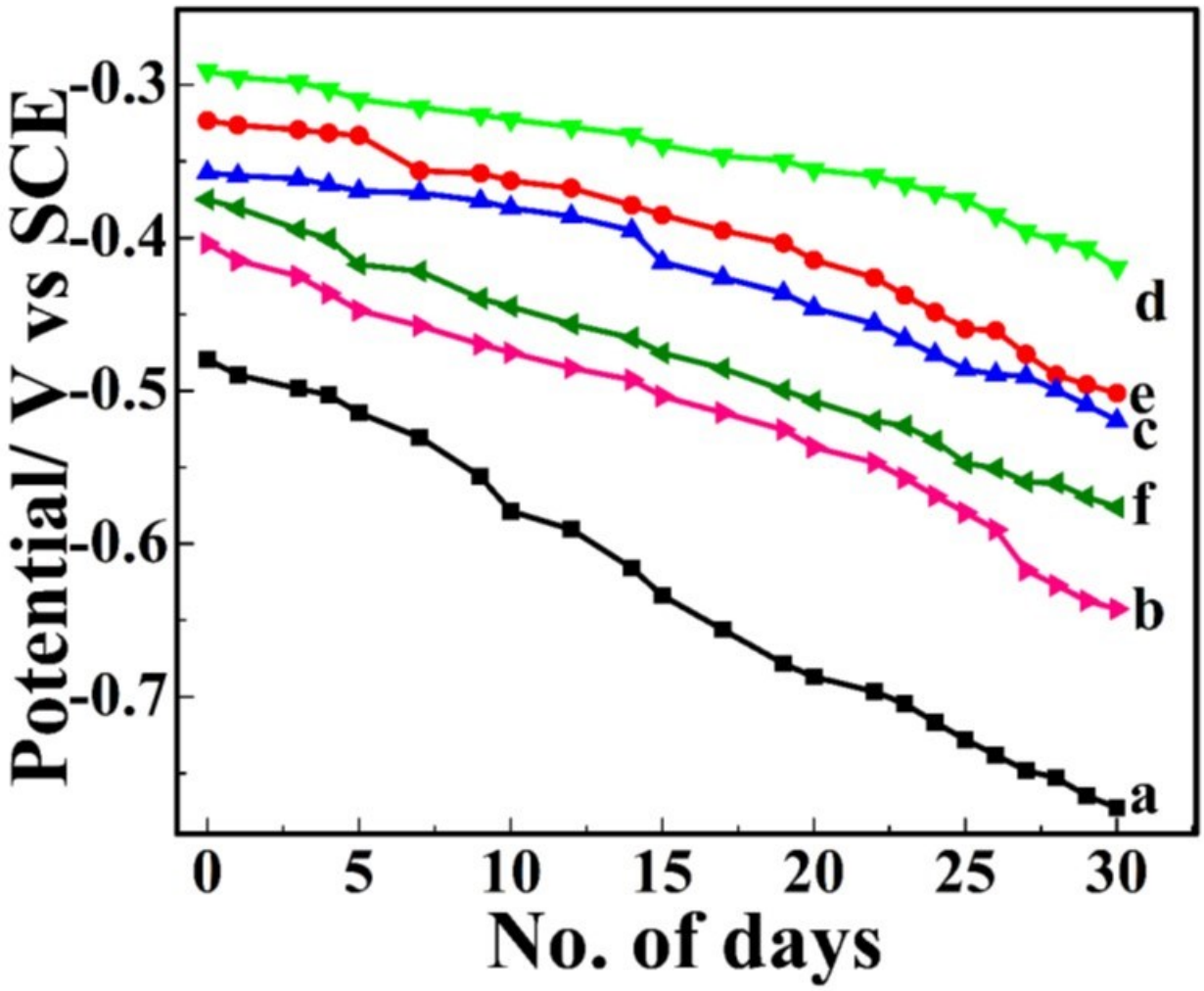

Fig. S14: The trend in OCP variation of the developed electrodes in 1 M NaOH solution at 25 ºC for a period of 30 days: a) Bare NiP, b) Bare PANI, c) PANI/Fe_2O_3–1GL, d) PANI/Fe_2O_3–2GL, e) PANI/Fe_2O_3–5GL and f) PANI/Fe_2O_3–10GL

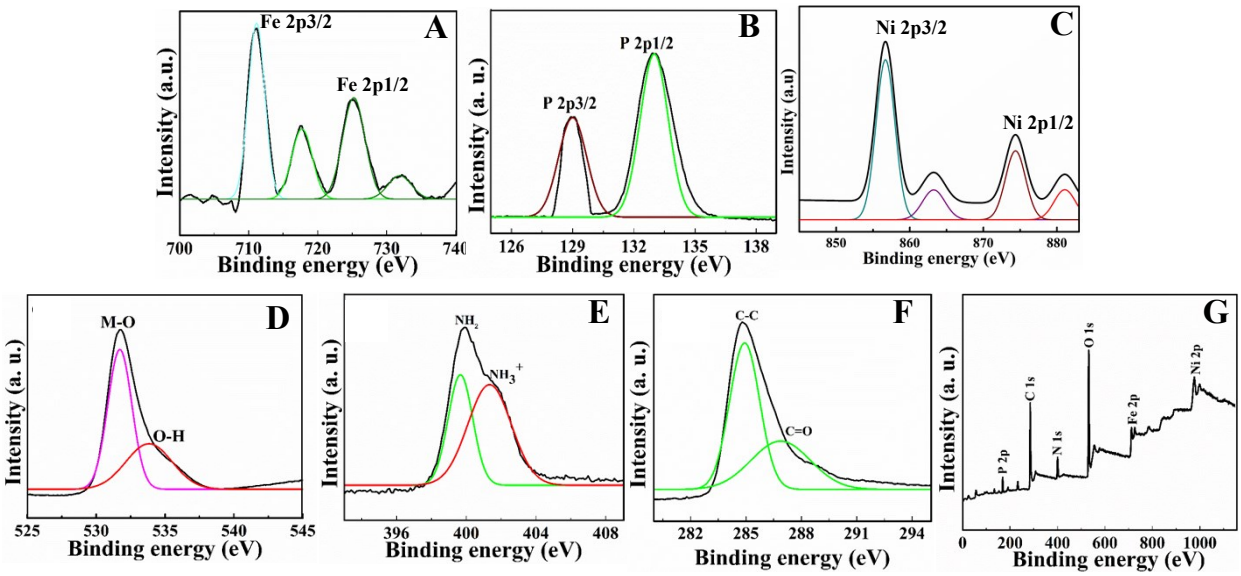

Fig. S15: X-ray photoelectron spectra of the tuned PANI/Fe_2O_3–2GL composite coating after long term HER study through chronopotentiometric analysis: **A**) Fe 2p, **B**) P 2p, **C**) Ni 2p, **D**) O 1s, **E**) N 1s, **F**) C 1s and **G**) survey spectrum